International Journal of GEOMATE, Aug., 2021, Vol.21, Issue 84, pp.1-8
ISSN: 2186-2982 (P), 2186-2990 (O), Japan, DOI: https://doi.org/10.21660/2021.84.j2172
Geotechnique, Construction Materials and Environment

STUDY ON FAILURE MECHANISM OF PLAIN CONCRETE PIER WITH COLD JOINT DURING EARTHQUAKES

*Aiko Furukawa[1], Yuta Kawamatsu[1] and Junji Kiyono[1]

[1]Department of Urban Management, Kyoto University, Japan

*Corresponding Author, Received: 15 April 2021, Revised: 30 April 2021, Accepted: 12 June 2021

ABSTRACT: In Japan, plain concrete piers with no reinforcing bars are still in service, and their damages have been reported in past earthquakes. The typical failure is the damage to the concrete edge below the cold joint, and no damage has occurred to the concrete above the joint. To prevent damage in future earthquakes, it is essential to clarify the failure mechanism and clarify whether the concrete above the joint can also fail. In this paper, the finite element analysis of the plain concrete pier under two sinusoidal wave inputs with different frequencies was performed, and the failure mechanism was investigated. The results revealed that tensile failure is caused by friction force at the joint, and the direction of friction force changes depending on the input frequency. The friction force causes tensile stress at the concrete below the joint when the input frequency is low. Past earthquake damages to the concrete below the joint correspond to the case with the low input frequency. It was also found that the friction force causes tensile stress at the concrete above the joint when the input frequency is high. Therefore, it was found that the concrete above the joint can fail when a large earthquake with high frequency occurs. Finally, a shaking table test was conducted using a miniature model made of styrene foam, and the mechanism revealed by the finite element analysis was confirmed.

Keywords: Plain concrete pier, Cold joint, Earthquake failure mechanism, Finite element analysis, Shaking table test

1. INTRODUCTION

Plain concrete piers are concrete piers with no reinforcing bars. In Japanese railway bridges, plain concrete piers were constructed before the design standards for RC bridges were stipulated in 1941 [1]. Even at present, many plain concrete piers are still in service. However, it has been reported that damages occurred to plain concrete piers during past earthquakes [2-4]. As shown in Fig. 1, typical damage is the horizontal displacement at the cold joint and the failure of the concrete edge below the joint. When the horizontal displacement is too large, or the concrete edge below the joint is severely damaged, it may cause a severe accident such as bridge collapse. Therefore, it is essential to understand the failure mechanism of the plain concrete piers and propose appropriate reinforcing measures for upcoming earthquakes.

Several studies have been done regarding the reinforcing methods. Reinforcement methods by winding with a steel plate [5], attaching RC reinforcement only to the part where seismic performance is insufficient [6], inserting steel rods [7], and using FRP and steel plate [8] have been studied by the static loading tests.

The researches regarding the failure mechanism of plain concrete piers are still few. In 2015, West Japan Railway Co., Ltd. conducted a shaking table test of a scaled plain concrete pier [9, 10]. The concrete edge below the joint was broken, and the failure shown in Fig. 1 was observed. However, no research has been made as to why the failure occurred only under the joint and whether there is any possibility of failure above the joint.

The researches by numerical analysis also have been conducted. Since the seismic behavior of plain concrete piers is highly nonlinear, including sliding and rocking phenomena, the numerical analysis based on the distinct element method (DEM) was conducted [11-14]. However, since the accuracy of stress and strain is not high in the DEM, understanding the failure mechanism was difficult.

The finite element method (FEM) is a numerical analysis method based on continuum mechanics, and the accuracy of stress and strain is higher than that of the DEM. However, the original FEM could not deal with the discrete deformable bodies since it is an analysis method for continuum. Recently, it is possible to simulate the nonlinear behavior of the discrete deformable bodies by the FEM using the contact analysis function.

Therefore, in this study, the numerical analysis of a plain concrete pier was performed using the contact analysis function of the finite element

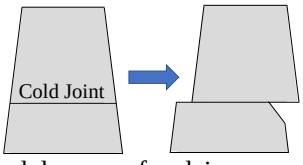

Fig. 1 Typical damage of a plain concrete pier

(a)Photo

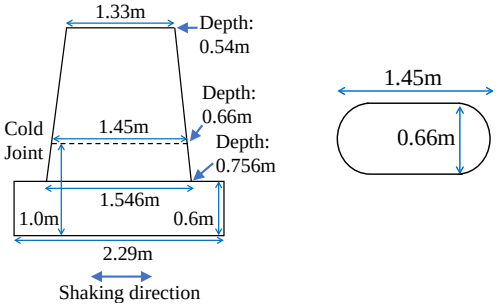

(b) Front view (concrete part only)

(c) Cross-section at the joint

Fig. 2 Target structure [9]

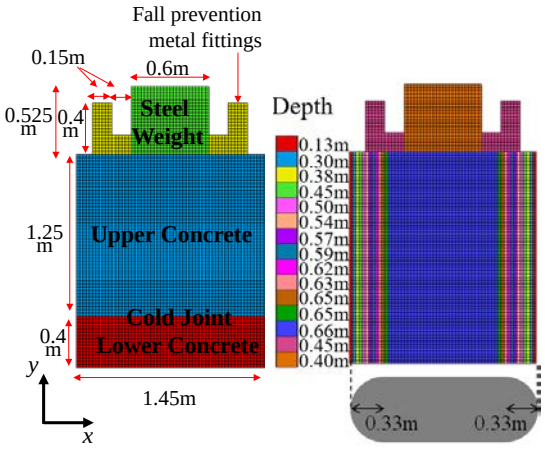

(a) Size

(b) Depth

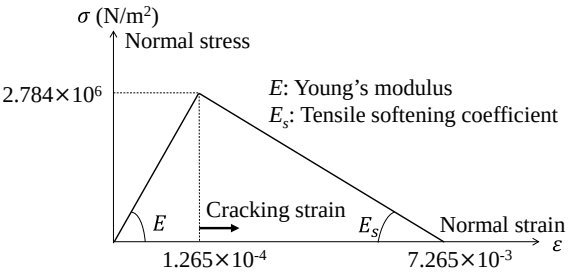

(c) Stress-strain relationship of concrete (tension)

Fig. 3 Analysis model

analysis software, MSC Marc [15]. This study aims to clarify the failure mechanism of plain concrete piers during earthquakes and to clarify whether the concrete edge above the joint can fail.

The shaking table test was also conducted using the miniature model of a plain concrete pier and confirmed whether the same tendency with the numerical analysis could be obtained.

Table 1 Analysis parameters

Value	Concrete	Steel weight/ fall-prevention metal fitting	Cold joint
Density(kg/m^3)	2.3×10^3	4.045×10^3	—
Young's modulus(N/m^2)	2.2×10^{10}	2.0×10^{11}	—
Poisson's ratio	0.20	0.30	—
Tensile strength(N/m^2)	2.784×10^6	—	—
Friction coefficient	—	—	0.64

2. FINITE ELEMENT ANALYSIS

2.1 Target Structure [9]

The target structure is a test specimen of a plain concrete pier used in the shaking table test [9, 10] (Fig. 2(a)). The specimen is a 1/2.5 scale model of the 14P pier of Uonogawa Bridge damaged during the 2004 Niigata-ken Chuetsu Earthquake.

Fig.2(b) shows the size of the specimen. The cross-sectional area of the pier decreases toward the top. Fig.2(c) shows the cross-section at the joint, which is a rectangle with a semi-circle at both sides.

2.2 Analysis Model

2.2.1 Size

The analysis model is shown in Fig. 3(a)(b). The *x*-axis is the excitation direction, and the *y*-axis is the vertical direction. The two-dimensional model was constructed with plane stress elements. Each element has a size of 2.5cm×2.5cm. The cross-section of the actual pier decreases toward the top, but for simplicity, the cross-section was set constant, and the cross-section at the joint (Fig.2(c)) was used as the representative. The semi-circle shape at both sides was expressed by setting the depth.

2.2.2 Analysis parameters [9]

Table 1 shows the analysis parameters.

As for concrete, values obtained by the element tests were used for density, Young's modulus, and tensile strength, and the general value was used for Poisson's ratio. Concrete was assumed to be elastoplastic, and the tension-softening constitutive law shown in Fig. 3 (c) was used.

As for steel weight and fall-prevention metal fittings, the general values for steel were used for Young's modulus and Poisson's ratio and assumed linear elastic. Density was obtained so that the total weight becomes similar between the test specimen and the analysis model.

The mass matrix of each element was computed based on the density, the element size of 2.5cm× 2.5cm, and the thickness shown in Fig.3(b).

The friction coefficient at the joint was set to 0.64, which was obtained from the test specimen. The concrete above the joint was pulled horizontally with a hydraulic jack and the load when it started sliding was measured by a load cell.

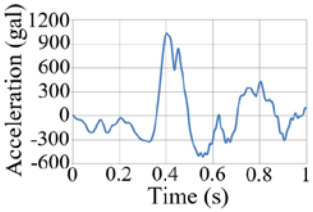

Fig. 4 Input acceleration used in shaking table test

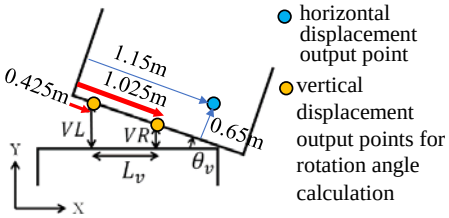

Fig. 5 Displacement output points

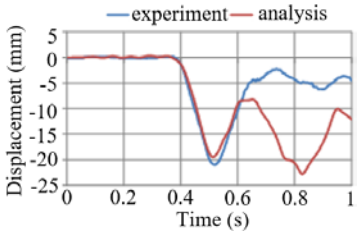

(a) Horizontal displacement

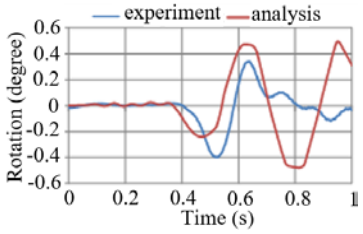

(b) Rotation angle

Fig. 6 Comparison of experimental and analysis results

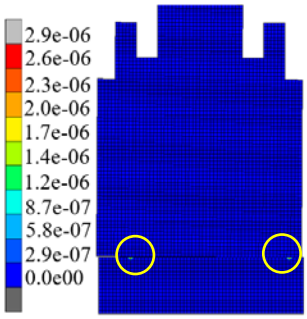

Fig. 7 The maximum principal value of cracking strain (The yellow circles indicate the crack occurrence position.)

2.3 Verification of Analysis Method

2.3.1 Input acceleration

First, the reproduction analysis of the shaking table test was performed, and the validity of the analysis method was confirmed by comparing the experimental and analysis results.

In the shaking table test [9], the input acceleration waveform was created by applying the scaling law to the design ground motion (L2, spectrum II, G2) for railway structures in Japan [16]. The amplitude of the input acceleration was gradually increased, and concrete below the joint was broken at both edges when the maximum input acceleration was 1000 gal. Therefore, the numerical analysis was performed for this case.

The acceleration waveform measured on the shaking table was input. To shorten the analysis time, acceleration data for one second, including the maximum amplitude, was used (Fig. 4) [9].

2.3.2 Comparison of experimental and analysis results

The horizontal displacement and rotation angle of the concrete above the joint was compared as shown in Fig. 6.

Horizontal displacement at the position indicated by the blue point in Fig. 5 was used as the horizontal displacement above the joint. The rotation angle was calculated by the following equation using vertical displacements *VL* and *VR* at two points indicated by the orange points in Fig. 5. The distance between the two orange points is L_v.

$$\theta_v = tan^{-1}\{(VL - VR)/L_v\} \quad (1)$$

The horizontal displacement is positive in the *x*-axis direction, and the rotation angle is positive in the clockwise direction.

From Fig. 6(a), the analysis and experimental results of horizontal displacement showed good agreement until 0.61 sec. The reason why they showed different behavior after 0.61 sec is as follows. The concrete edge below the joint was broken, and concrete pieces fell at 0.61 sec in the experiment. In contrast, the falling of the concrete pieces was not considered in the analysis. Therefore, the behavior after the falling of concrete pieces was not reproduced. However, the displacement history up to 0.61 sec could be reproduced accurately.

On the other hand, the reproduction accuracy of the rotation angle (Fig. 6(b)) was lower than that of horizontal displacement. The authors' tried to improve the analysis model, but the rotation angle could not be reproduced as accurately as the horizontal displacement. The current model is the most reproducible among those we have achieved.

Finally, Fig. 7 shows the maximum principal value of the cracking strain at 0.61 sec. Cracking strain is defined as the strain that exceeds the tensile strength. The tensile failure occurred at two locations near the left and right edges, consistent with the shaking table test result.

Since it is confirmed that horizontal displacement and the occurrence of the failure can be reproduced by the numerical analysis, further investigation is performed.

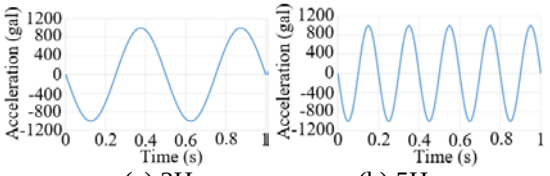

(a) 2Hz (b) 5Hz

Fig. 8 Input acceleration of sine wave

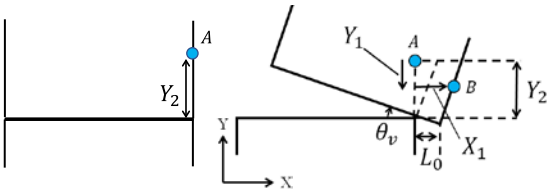

(a) Initial state (b) State during excitation

Fig. 9 Calculation of pure relative displacement L_0 from horizontal displacement X_1 and vertical displacement Y_1.

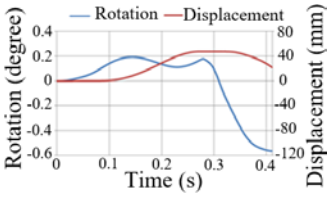

(a)Pure horizontal displacement and rotation angle

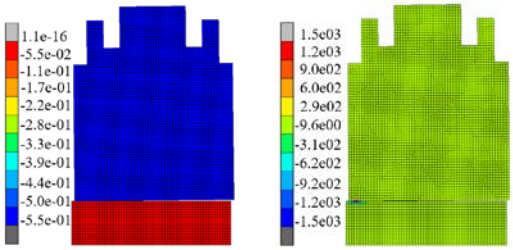

(b)Horizontal velocity (0.4sec) (c)Friction force (0.4sec)

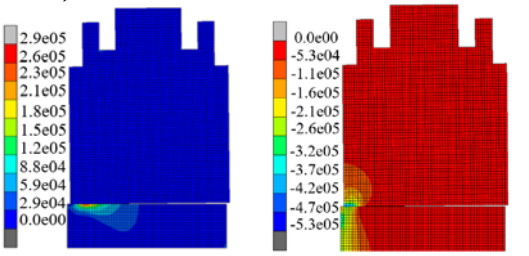

(d)Maximum principal value of stress (0.4sec) (e)Minimum principal value of stress (0.4sec)

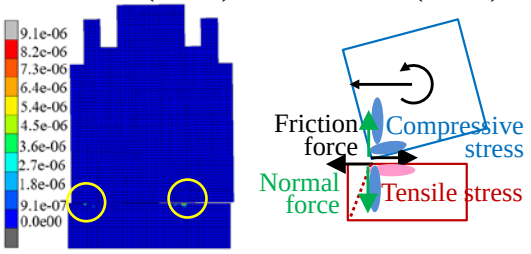

(f)Maximum principal value of cracking strain (0.4sec) (g) Failure mechanism

Fig. 10 Analysis results for 2 Hz input

2.4 Investigation of Failure Mechanism

2.4.1 Input accelerations

Two types of a sine wave of 1000 gal with different frequencies of 2Hz and 5Hz were input (Fig. 8).

The rotation angle was obtained by Eq. (1) from the vertical displacement at orange points in Fig. 5. As for the horizontal displacement, pure horizontal displacement was calculated by removing the horizontal displacement due to rotation. As shown in Fig. 9, it is assumed that the node located at point A before analysis moves to point B due to sliding and rotation. Let X_1 be displacement in the positive direction of the *x*-axis and Y_1 be displacement in the negative direction of the *y*-axis at this time, and let Y_2 (=0.65m) be the distance from the joint to point A. Pure horizontal displacement L_0 was calculated by the following equation.

$$L_0 = \{X_1 - (Y_2 + Y_1)tan\theta_v\}cos^2\theta_v \qquad (2)$$

2.4.2 Analysis results for 2 Hz input

Analysis results are shown in Fig. 10. Fig.10(a) shows the pure horizontal displacement and rotation angle above the joint. At 0.4 sec, a failure occurred at the left edge of the concrete below the joint. After the failure, the solution became unstable and terminated at 0.41 sec.

Fig.10(a) indicates that the concrete above the joint slid in the negative direction while rotating counterclockwise at 0.4 sec when the failure occurred. Fig. 10(b) is the horizontal velocity at 0.4 sec. It also shows the concrete above the joint rotated counterclockwise and slid in the negative direction of the *x*-axis (left side) since the velocity is negative. Fig. 10(c) is friction force at 0.4 sec. It shows that positive (rightward) friction force was generated on the concrete above the joint, and negative (leftward) friction force was generated on the concrete below the joint because the upper body slid in the negative direction.

Figures. 10 (d) and (e) are the maximum (tensile) and minimum (compressive) principal value of stress at 0.4 sec. Fig. 10 (f) shows the maximum principal value of cracking strain at 0.4 sec.At the left concrete edge below the joint, tensile stress was generated (Fig.10(d)) due to friction force (Fig.10(c)), and the compressive stress was also generated in the outer side (Fig.10(e)) due to the weight of the concrete above the joint. The area where the tensile stress is generated got cracked (Fig.10(f)). Therefore, the cause of the tensile failure is the friction force.

At the left concrete edge above the joint, only compressive stress occurred (Fig.10(e)). Both the friction and the reaction force against the weight caused the compressive stress. Therefore, no tensile failure occurred on the concrete above the joint.

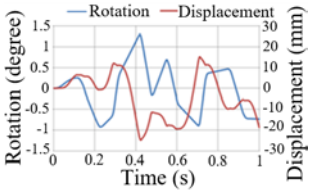

(a)Pure horizontal displacement and rotation angle

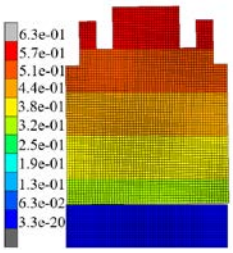

(b)Horizontal velocity (0.28sec)

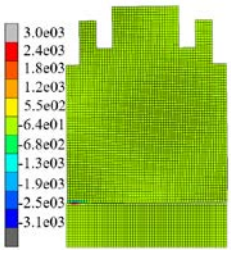

(c)Friction force (0.28sec)

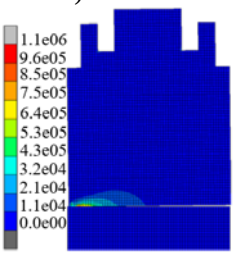

(d)Maximum principal value of stress (0.28sec)

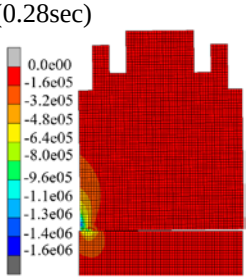

(e)Minimum principal value of stress (0.28sec)

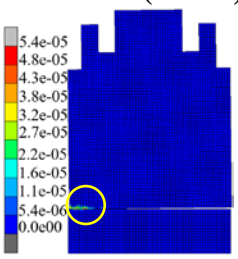

(f)Maximum principal value of cracking strain (0.28sec)

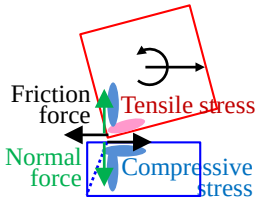

(g) Failure mechanism

Fig. 11 Analysis results for 5Hz input

Fig. 10 (f) shows that there are two cracks on the concrete below the joint. The crack in the right that occurred at 0.13 sec remained unclosed, and the left one occurred at 0.4 sec. These cracks were caused by tensile stress generated by friction force.

2.4.3 Failure mechanism due to 2 Hz input

The failure mechanism is shown in Fig. 10 (g). When the upper concrete slides in the same direction as rotation, tensile stress is generated below the joint by friction force. When tensile stress exceeds the tensile strength, tensile failure occurs. The above is the failure mechanism of the concrete below the joint. No tensile failure occurs on the upper concrete because the friction force generates the compressive stress.

2.4.4 Analysis results for 5Hz input

Analysis results are shown in Fig. 11. Fig. 11 (a) shows the time history of the pure horizontal displacement and rotation angle above the joint. At 0.28 sec, a tensile failure occurred on the concrete above the joint. Since tensile failure above the joint had not been reported in past earthquakes, the mechanism is considered.

Fig. 11(a) shows that the concrete above the joint slid to the right while rotating counterclockwise at 0.28 sec. Fig. 11(b) is the horizontal velocity at 0.28 sec. It also shows that the concrete above the joint slid in the positive direction (right side) of the *x*-axis while rotating counterclockwise. Fig. 11(c) is friction force at 0.28 sec. It shows negative (leftward) friction force was generated on the concrete above the joint, and positive (rightward) friction force was generated on the concrete below the joint because the upper body slid in the positive direction.

Figs. 11 (d) and (e) are the maximum (tensile) and minimum (compressive) principal value of stress at 0.28 sec. Fig. 11 (f) shows the maximum principal value of cracking strain at 0.28 sec.

At the left concrete edge above the joint, tensile stress was generated (Fig.11(d)) due to friction force (Fig.11(c)), and the compressive stress was also generated in the outer side (Fig.11(e)) due to the reaction force against the weight of the concrete above the joint. The area where the tensile stress is generated got failed in the analysis (Fig.11(f)). Therefore, the cause of the tensile failure is the friction force.

At the left concrete edge below the joint, only compressive stress occurred (Fig.11(e)). Both the friction force and the weight of the upper body caused the compressive stress. Therefore, no tensile failure occurred on the concrete below the joint.

2.4.5 Failure mechanism due to 5 Hz input

The failure mechanism is shown in Fig. 11 (g). When the upper concrete slides opposite to rotation, tensile stress is generated above the joint by friction force. When tensile stress exceeds the tensile strength, tensile failure occurs. The above is the failure mechanism of the concrete above the joint.

2.4.6 Influence of input frequency

Why did the upper concrete slide in the same direction as rotation in 2Hz and the opposite direction in 5Hz? It might be due to the relationship between the predominant frequency of rocking and the input frequency.

To confirm this hypothesis, sine waves of 1000 gal with various frequencies were input to the analysis model. The frequency was changed from 0.5Hz to 5.0Hz with an interval of 0.5Hz. It was found that the rotation angle was the largest when the input frequency was 3.5Hz. Similar phenomena to the case of 2 Hz were observed when the input frequency is lower than 3.5 Hz, and similar

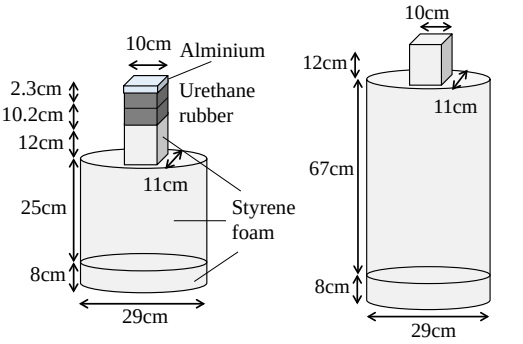

(a) Specimen size

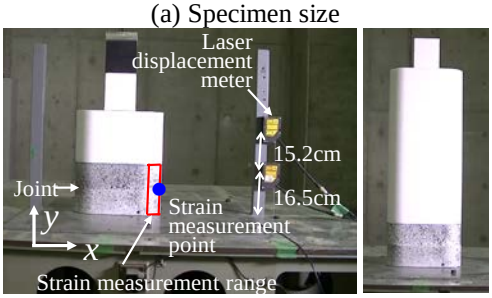

(b) Experimental setting

Fig. 12 Shaking table test specimen and experimental setting (left: specimen A, right: specimen B)

phenomena to the case of 5 Hz were observed when the input frequency is higher than 3.5 Hz.

In the forced vibration of a single-degree-of-freedom system, the input and output are in the same phase when a sine wave with a frequency lower than the natural frequency is input. The input and output have the opposite phase when a sine wave with a frequency higher than the natural frequency is input. Thus, the upper concrete slides in the same direction as rotation when the input frequency is lower than the predominant frequency of rocking. The upper concrete may slide in the opposite direction to the rotation when the input frequency is higher than the predominant frequency of rocking.

However, damage to the upper concrete has not been reported in past earthquakes. It is probably because the large earthquake whose predominant frequency is higher than the rocking frequency of the upper body is rare. Further study is necessary to clarify the influence of input frequency.

3. SHAKING TABLE TEST

3.1 Specimen Overview

A shaking table test was conducted to confirm the aforementioned tensile stress occurring mechanism. Two types of specimens were prepared as shown in Fig. 12 (a). The dimension of specimen A was determined so that it is about 1/12.5 scale of 14P pier of Uonogawa Bridge, which was damaged during the 2004 Niigata-ken Chuetsu Earthquake. Specimen B is a model in which the height of specimen A is lengthened. Urethane rubber and aluminum pieces were placed on specimen A to increase the weight (Fig.12(a)). The lower body, the upper body, and the weight of specimen A are 0.064kg, 0.20kg, and 2.3kg, respectively. And those of specimen B are 0.064kg, 0.51kg, and 0.031kg, respectively.

To measure the strain of the specimen by the image measurement, the specimens were made of styrene foam, which had low rigidity and was easily deformed compared to concrete. Young's modulus of the styrene foam was 8.9×10^6 N/m^2 and the friction coefficient at the joint was 0.48.

3.2 Experimental Setting

Fig. 12 (b) shows the specimen installed on the shaking table. Columns were installed on the shaking table, and laser displacement meters were installed at two different heights to measure horizontal relative displacement. From these horizontal relative displacements at two heights, the pure horizontal displacement and rotation angle were calculated. The acceleration of the shaking table was measured by an accelerometer installed on the shaking table. The measurement time interval is 1.0×10^{-3} sec.

The strain at the right end of the joint was measured by image measurement using two high-speed cameras and the digital image correlation system [17]. A spray was applied to the specimen to make spots. The movement of the spots was traced and the strain was computed. The shooting time interval was 1.5625×10^{-3} sec.

3.3 Input Acceleration

For specimen A, sinusoidal acceleration with 3.5Hz, which is lower than the predominant frequency of rocking, was input. For specimen B, sinusoidal acceleration with 5.0Hz, which is higher than the predominant frequency of rocking, was input. They were input in the *x*-axis direction. Due to the nature of the shaking table, the amplitude of the input acceleration gradually increased and finally reached about 1000 gal for specimen A and about 600 gal for specimen B.

3.4 Result

3.4.1 Specimen A (3.5Hz)

Fig. 13 (a) shows the acceleration history measured on the shaking table. Fig. 13 (b) shows the time history of the pure horizontal displacement and rotation angle above the joint. Pure horizontal displacement and rotation angle seem almost in the same phase. The fact that horizontal displacement occurred at about 0.6 sec means the input acceleration amplitude gradually increased, and sliding started at about 0.6 sec when the inertia force exceeded the friction force.

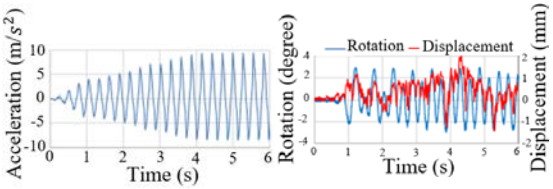

(a) Input acceleration (b) Pure horizontal displacement and rotation angle

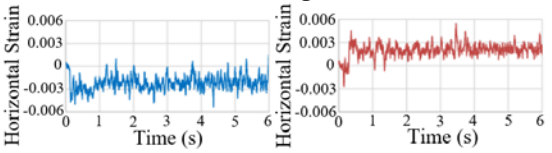

(c) Horizontal strain above the joint (d) Horizontal strain below the joint

Fig. 13. Results of shaking table test (specimen A)

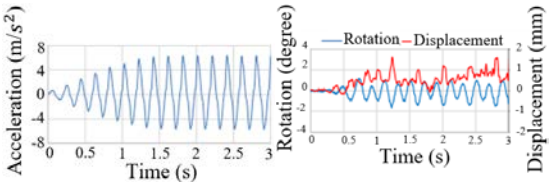

(a) Input acceleration (b) Pure horizontal displacement and rotation angle

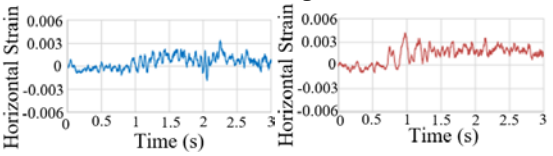

(c) Horizontal strain above the joint (d) Horizontal strain below the joint

Fig.14. Results of shaking table test (specimen B)

Figure. 13 (c)(d) shows horizontal strain above and below the joint. The tension strain is positive. Compressive strain mainly occurred at the body above the joint, and tensile strain mainly occurred at the lower body. It is the same tendency with the case of 2 Hz input in the analysis.

3.4.2 Specimen B (5Hz)

Figure. 14 (a) shows the acceleration history measured on the shaking table. Fig. 14 (b) shows the time history of the pure horizontal displacement and rotation angle above the joint. Pure horizontal displacement and the rotation angle are almost in the opposite phases.

Figure. 14 (c)(d) shows horizontal strain above and below the joint. In the body above the joint, tensile strain occurred after 1 sec. It is the same tendency with the case of 5 Hz input in the analysis.

On the other hand, the tensile strain also occurred on the body below the joint after 0.8 sec. The reason for this could not be clarified. However, the tensile strain may be generated by the collision force from the upper body and Poisson's effect.

This study used styrene foam since it is more likely to be deformed with small stress. Therefore, it was possible to measure the strain by the image measurement. However, residual deformation is more likely to remain than concrete, so it is necessary to study further using concrete specimens.

4. CONCLUSION

This study investigated the failure mechanism of plain concrete piers during earthquakes.

First, the finite element analysis was conducted, and the failure mechanism was clarified as follows.

The typical damage observed during the earthquake is the failure of the concrete edge under the joint. This damage was found to be caused by the friction force at the joint. When the input frequency is low, the concrete above the joint slides in the same direction as rotation, and tensile stress is generated at the concrete edge below the joint by friction force. When tensile stress exceeds the tensile strength, tensile failure occurs. This is the failure mechanism of the concrete edge below the joint. No tensile failure occurs on the upper concrete because the compressive stress is generated by the friction force.

In the past earthquakes, no damage has been reported in the concrete above the joint. However, it was found that the damage can also occur at the concrete above the joint. When the input frequency is high, the upper concrete slides in the direction opposite to rotation, and tensile stress is generated above the joint by friction force. When tensile stress exceeds the tensile strength, tensile failure occurs. This is the failure mechanism of the concrete above the joint.

The shaking table test was also conducted to confirm whether the aforementioned tensile stress occurrence mechanism can be observed. The strain was measured instead of the stress. When the input frequency was low, the tensile strain occurred at the lower body, and the compressive strain occurred at the upper body. This is the same mechanism observed in the finite element analysis.

When the input frequency was high, the tensile strain occurred at the upper body, and this is the same mechanism observed in the finite element analysis. However, the tensile strain also occurred at the lower body, and this reason could not be clarified in this study. However, the tensile strain may be generated by the collision force from the upper body and Poisson's effect. Further investigation is necessary.

Since this study used styrene foam, the residual deformation is more likely to remain than concrete. Therefore, it is necessary to study further using concrete specimens.

5. ACKNOWLEDGMENT

We would like to express our sincere appreciation to West Japan Railway Company for providing the shaking table test results. We would also like to thank Professor Shiotani and Professor Hashimoto from Kyoto University for allowing us to use the digital correlation systems.

6. REFERENCES

[1] Yamada, M., Reinforced mixed soil bridge design tips, Civil Engineering Co., Ltd., Civil and architectural engineering, Vol.1, Issue 7-8, 1914. (in Japanese)

[2] Hakuno, M., Fujino, Y., Katada, T., and Matsubara, K., Damage survey report of Miyagiken-oki Earthquake in 1978 – Mainly related to civil engineering. Bulletin of the Earthquake Research Institute, University of Tokyo, Vol.54, 1979, pp.351-398. (in Japanese)

[3] Morikawa, H., and Fukushima, Y., Damage to civil engineering structures due to the 2004 Niigata-ken Chuetsu Earthquake. Research reports on earthquake engineering, Center for Urban Earthquake Engineering, Tokyo Institute of Technology, No.92, 2004, pp.43-56. (in Japanese)

[4] Kyushu Institute of Technology Disaster Research Team, The 2004 Niigata-ken Chuetsu Earthquake –Second damage investigation bulletin version, http://www.civil.kyutech.ac.jp/pub/kosa/ijikenHP/tyuuetujisin20041025.pdf. [Accessed April 14, 2021.] (in Japanese)

[5] Sugisaki, H., Kobayashi, and K., Reversal cyclic loading test of plain concrete piers with construction joint retrofitted by RC. Proceedings of the Japan Concrete Institute, Vol.29, No.3, 2007, pp.1093-1098. (in Japanese)

[6] Suzuki, Y., Kobayashi, K., Experimental study on rational seismic strengthening method for plain concrete bridge piers. Proceedings of the Japan Concrete Institute, Vol.31, No.3, 2009, pp.1081-1086. (in Japanese)

[7] Tokunaga, M., Tadokoro, T., Tanimura, Y., Nishimura, A., Hoshi, H., Murata, Y., and Omoto S., The seismic strengthening effect of joints of plain concrete piers by inserting steel rods. The 64th JSCE Annual Meeting, Japan Society of Civil Engineers, V-484, 2009, pp.965-966. (in Japanese)

[8] Choi, E., Rhee, I., Park, J. and Cho, B.S., Seismic retrofit of plain concrete piers of railroad bridges using composite of FRP-steel plates. Composites Part B: Engineering, Vol.42, No.5, 2009, pp.993-1336. (in Japanese)

[9] Railway Technical Research Institute, Design standards for railway structures and commentary (Seismic design). Maruzen, 2012. (in Japanese)

[10] Railway Technical Research Institute, Report of contracted business from West Japan Railway Co., Ltd., A confirmation test of seismic measures for plain concrete piers, 2015. (in Japanese)

[11] Sakaoka, K., Otsubo, M., Wada, K., and Koyama, T., Experimental study on the seismic retrofit of plain concrete piers using the movement restraining devices for the construction joint, Journal of Japan Society of Civil Engineers, Ser, A1 (Structural Engineering & Earthquake Engineering), Vol.74, No.4, 2018, I_1-I_15. (in Japanese)

[12] Furukawa, A., Kiyono, J., and Toki, K., Proposal of a numerical simulation method for elastic, failure and collapse behaviors of structures and its application to seismic response analysis of masonry walls. Journal of Disaster Research, Vol.6, No.1, 2011.

[13] Furukawa, A, Mizukami, A., and Kiyono, J. Study on seismic damage occurrence mechanism for plain concrete pier of railroad bridge and seismic measures, Journal of Japan Society of Civil Engineers, Ser, A1 (Structural Engineering & Earthquake Engineering), Vol.72, No.4, 2016, pp. I_33-I_43. (in Japanese)

[14] Furukawa, A, Yoshikawa, H., and Kiyono, J., Dynamic behavior analysis of a plain concrete pier during shaking table test by using refined DEM, Journal of Japan Society of Civil Engineers, Ser, A1 (Structural Engineering & Earthquake Engineering), Vol.73, No.4, 2017, pp.I_32-I_47. (in Japanese)

[15] Furukawa, A., Yano, S., and Kiyono, J., Study on numerical analysis of failure behavior of a plain concrete pier during earthquake, Journal of Japan Society of Civil Engineers, Ser, A1 (Structural Engineering & Earthquake Engineering), Vol.74, No.4, 2018, pp.I_883-I_896. (in Japanese)

[16] MSC Software Corporation: Marc, https://www.mscsoftware.com/ja/product/marc. [Accessed April 14, 2021.]

[17] Correlated Solutions. The VIC3D System. http://correlatedsolutions.com/vic-3d/. [Accessed April 14, 2021.]